Anisotropic superconductivity in the topological crystalline metal $Pb_{1/3}TaS_2$ with multiple Dirac fermions

Xiaohui Yang,[1,2,*] Tonghua Yu,[3] Chenchao Xu,[3] Jialu Wang,[1,2] Wanghua Hu,[1,2] Zhuokai Xu,[1,2] Tao Wang,[1,2] Chao Zhang,[4] Zhi Ren,[1,2] Zhu-an Xu,[5,6] Motoaki Hirayama,[3,7] Ryotaro Arita,[3,7] and Xiao Lin[1,2,†]

[1]*Institute of Natural Sciences, Westlake Institute for Advanced Study, Hangzhou 310024, People's Republic of China*

[2]*Key Laboratory for Quantum Materials of Zhejiang Province, School of Science, Westlake University, Hangzhou 310024, People's Republic of China*

[3]*Department of Applied Physics, University of Tokyo, Tokyo 113-8656, Japan*

[4]*Instrumentation and Service Center for Physical Sciences, Westlake University, Hangzhou 310024, People's Republic of China*

[5]*Zhejiang Province Key Laboratory of Quantum Technology and Device, Department of Physics, Zhejiang University, Hangzhou 310027, People's Republic of China*

[6]*State Key Laboratory of Silicon Materials, Zhejiang University, Hangzhou 310027, People's Republic of China*

[7]*RIKEN Center for Emergent Matter Science, 2-1 Hirosawa, Wako, 351-0198, Japan*

(Received 31 May 2021; accepted 16 July 2021; published 28 July 2021)

Topological crystalline metals and semimetals (TCMs) have stimulated great research interest, which broadens the classification of topological phases and provides a valuable platform to explore topological superconductivity. Here, we report the discovery of superconductivity and topological features in Pb-intercalated transition-metal dichalcogenide $Pb_{1/3}TaS_2$. Systematic measurements indicate that $Pb_{1/3}TaS_2$ is a quasi-two-dimensional (q-2D) type-II superconductor ($T_c \approx 2.8$ K) with a significantly enhanced anisotropy of upper critical field ($\gamma_{H_{c2}} = H_{c2}^{ab}/H_{c2}^{c} \approx 17$). In addition, first-principles calculations reveal that $Pb_{1/3}TaS_2$ hosts multiple topological Dirac fermions in the electronic band structure. We discover four groups of Dirac nodal lines on the $k_z = \pi$ plane and two sets of Dirac points on the rotation or screw axes, which are protected by crystalline symmetries and robust against spin-orbit coupling (SOC). Dirac-cone-like surface states emerge on the (001) surface because of band inversion. Our work shows that the TCM candidate $Pb_{1/3}TaS_2$ is a promising arena to study the interplay between superconductivity and topological Dirac fermions.

DOI: 10.1103/PhysRevB.104.035157

I. INTRODUCTION

The search for exotic topological phases of condensed matter has attracted significant attention since the discovery of topological insulators (TIs), a unique class of electronic systems that show insulating bulks and topologically protected boundary excitations [1–9]. Shortly following TIs, topological metals and semimetals (TSMs) with bulk band crossings close to the Fermi level were broadly proposed and verified [10–18]. Because of the topological bulk and surface states, for instance, nodal-line metals and semimetals (NLSMs) exhibit unconventional transport features, such as three-dimensional quantum Hall effect and high-temperature surface superconductivity [19,20]. In the absence of magnetism, a centrosymmetric TSM, where both spatial inversion ($\mathcal{P}$) and time-reversal ($\mathcal{T}$) symmetries are preserved, may host quadruply degenerate bulk nodes resembling massless Dirac fermions [11,13]. Compared with the noncentrosymmetric case, however, these degeneracies are unstable under significant spin-orbit coupling (SOC) unless extra crystalline symmetries are present [10]. To be more specific, apart from the $\mathcal{PT}$ protection, a stable Dirac nodal point entails the guarantee of a rotation or screw symmetry [11,13], and a Dirac nodal line can be supported by additional nonsymmorphic operations [21–24]. Crystalline symmetries are therefore an essential factor for the search of TSMs hosting stable bulk Dirac fermions. We alternatively refer to such TSMs as topological crystalline metals and semimetals (TCMs) [25].

Recently, the family of the so-called 112 systems, MTX_2 (M = Pb, Sn, Tl or In, T = Ta or Nb, X = Se or S), has created a surge of research activities, because of their superconductivity and rich topological nature [26–30]. The noncentrosymmetric $PbTaSe_2$ (derived from $1H$-$TaSe_2$ by intercalating Pb in the van der Waals gap) was reported to be a promising topological superconductor (TSC) candidate, due to the observation of zero-energy Majorana bound states in the vortices [31]. $PbTaSe_2$ is also a typical NLSM where the nodal lines are guaranteed by mirror symmetry [8]. Another group of 112-type compounds host centrosymmetric lattice, including $PbTaS_2$ [32] and $SnTaS_2$ [33]. In these compounds, the nodal lines are protected by the $\mathcal{PT}$ symmetry in absence of SOC and is fragile under strong SOC [33].

Herein, based on symmetry analysis and band calculations, we predict another TCM candidate, the centrosymmetric crystal $Pb_{1/3}TaS_2$, which hosts multiple stable nodal point and line structures. In contrast to the above-mentioned 112 systems,

*yangxiaohui@westlake.edu.cn
†linxiao@westlake.edu.cn

nodal lines in $Pb_{1/3}TaS_2$ are robust against SOC by virtue of the nonsymmorphic symmetry. Dirac points are furthermore unveiled, stabilized by rotation and screw symmetries. Band inversion gives rise to Dirac-cone-like surface states in the (001) surface. In addition, we synthesize and characterize this single crystal in an experiment. The results show that $Pb_{1/3}TaS_2$ peculiarly exhibits quasi-two-dimensional (q-2D) superconductivity ($T_c = 2.8$ K) with large anisotropy in upper critical field H_{c2}. Consequently, the superconductor $Pb_{1/3}TaS_2$ is a unique electronic system manifesting versatile nontrivial topological nature, offering a realistic material test bed for the exploration of the Dirac fermions and even possible TSC.

II. METHODS

The $Pb_{1/3}TaS_2$ single crystals were prepared by the chemical vapor transport method. Stoichiometric amounts of high-purity Pb, Ta, and S powders with the transport agents $PbBr_2$ (10 mg/cm^3 in concentration) were thoroughly mixed and sealed in an evacuated quartz tube. The tube was heated at 1173 K with a temperature gradient of 5 K/cm for one week in a two-zone furnace.

The x-ray diffraction (XRD) pattern was performed on a Bruker D8 Advance x-ray diffractometer with Cu-K_α radiation. The chemical composition was determined by an energy-dispersive x-ray (EDX) spectrometer (Model Octane Plus) affiliated to a Zeiss Gemini 450 Schottky field emission scanning electron microscope (SEM). The transport measurements were measured on an Oxford superconducting magnet system equipped with a ^{3}He cryostat. The DC magnetization was carried out on a Quantum Design magnetic property measurement system (MPMS3).

The density functional theory (DFT) calculations are performed using the Vienna *ab initio* simulation package (VASP) [34], based on the generalized gradient approximation (GGA) method under the Perdew-Burke-Ernzerhoff (PBE) parametrization [35]. The energy cutoff of the plane wave is 323.4 eV. The Brillouin zone (BZ) is sampled by a 12 × 12 × 4 grid for the self-consistent calculations. Irreducible representations (IRs) of electronic eigenstates at high-symmetry k points are determined via an in-house code and the software package `irvsp` [36]. Wannier functions are constructed by projecting Bloch states onto Ta 5d orbitals through WANNIER90 [37–39] without the iterative maximal localization procedure. Nodal lines or points and surface spectrum are computed with the WANNIERTOOLS package [40], where the latter is based on the iterative Green's function method [41]. Pre- and postprocessing tools and utilities for solids computation [42–45] are exploited.

III. RESULTS AND DISCUSSION

$Pb_{1/3}TaS_2$ crystallizes in the centrosymmetric hexagonal space group $P6_3/mcm$ (no. 193), with the lattice constants $a = b = 5.76$ Å, $c = 14.81$ Å [46]. As illustrated in Fig. 1(a), Ta atoms are in trigonal-prismatic coordination by S atoms and the stacking sequence of S-Ta-S sandwiches follows that in 2H-TaS_2 [47]. Pb atoms are intercalated in between TaS_2 layers, but the occupation number is only one third of that in 112 $PbTaS_2$ phase [32]. Moreover, Pb ions sit on top of Ta sites, distinct from the 112 phase, in which Pb sits on top of S sites. Figure 1(b) presents the XRD pattern of $Pb_{1/3}TaS_2$ single crystals normal to the *ab* plane. The inset shows the full width at half-maximum (FWHM) of the (0010) peak is only 0.04°, indicating the high crystalline quality. The interplanar spacing is calculated to be 14.84 Å, similar to previous report [46]. According to the EDX data (see Fig. S1 of the Supplemental Material [48]), the molar ratio of Pb, Ta, and S atoms amounts to 1:3:6, in good agreement with the nominal one.

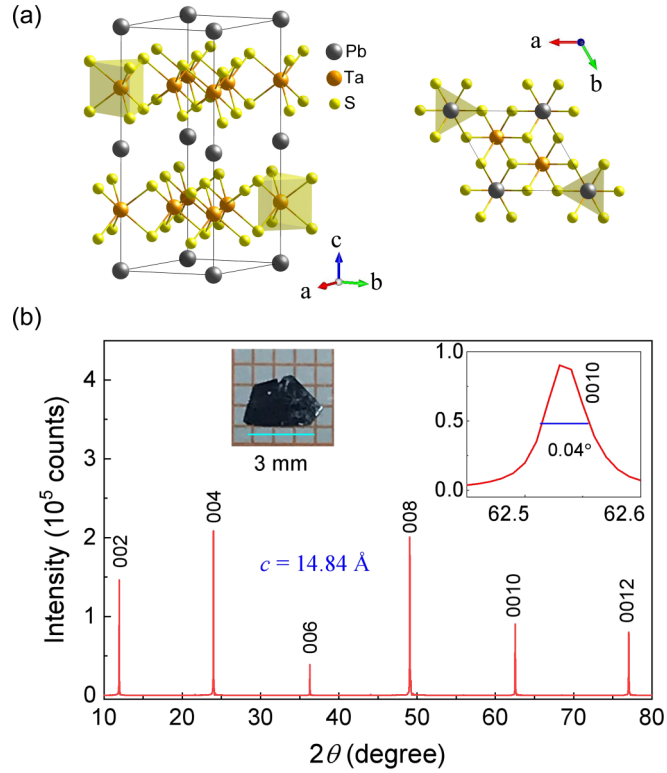

FIG. 1. (a) The crystal structure of $Pb_{1/3}TaS_2$ along different directions. (b) XRD pattern of the single crystal with (00l) reflections; the inset of the right panel enlarges the (0010) reflection.

Figure 2(a) shows the in-plane resistivity ρ_{ab} as a function of temperature T for $Pb_{1/3}TaS_2$, which exhibits metallic behavior with a high residual resistivity ratio [$RRR = \rho(300K)/\rho(3\ K)$] amounting to 24. The enlarged figure in the inset of Fig. 2(a) shows a sharp superconducting transition, $T_c^{50\%}$ of which determined at the half value of the normal state resistivity is around 2.8 K, higher than 2H-TaS_2 (T_c = 0.8 K) [49] and $PbTaS_2$ (T_c = 2.6 K) [32]. Figure 2(b) shows the T dependence of dc magnetic susceptibility with an external magnetic field (H = 2 Oe) along the *ab* plane. The diamagnetic signal reveals a superconducting transition at 2.7 K in consistent with transport measurements. The shielding volume fraction of superconductivity is close to 100% from the zero-field cooling (ZFC) process.

The Hall data ρ_{yx} at different temperatures are presented in Fig. 2(c). ρ_{yx} is positive and linear in field, which suggests holes dominate in charge transport. The inset of Fig. 2(c) presents the Hall coefficient $R_H = \rho_{yx}/H$, which varies slowly with T. Note that the carrier concentration n cannot be directly

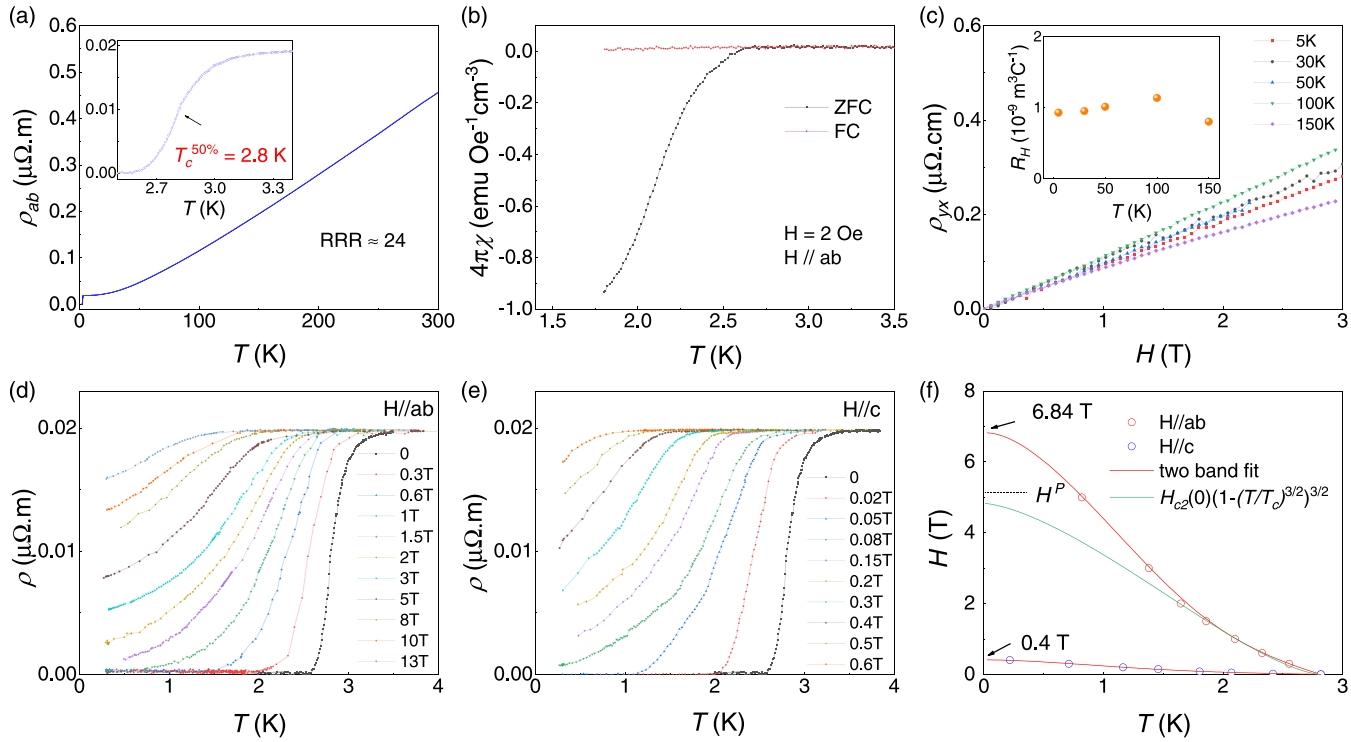

FIG. 2. (a) T dependence of the electrical resistivity ρ_{ab} of $Pb_{1/3}TaS_2$ single crystal. The inset shows the superconducting transition around T_c. (b) T dependence of dc magnetic susceptibility ($H//ab$, $H = 2$ Oe) around T_c. (c) Magnetic field dependence of Hall resistivity for $Pb_{1/3}TaS_2$ at different temperatures. Inset: the Hall coefficient vs temperature. [(d), (e)] The low T resistivity under different magnetic fields of single crystal parallel and perpendicular to the ab plane, respectively. (f) T dependence of the H_{c2} with two-band fits for both directions; the black line dictates the Pauli paramagnetic limit.

deduced from R_H given the multiband nature of $Pb_{1/3}TaS_2$ (see the band structure below).

Figures 2(d) and 2(e) show the T-dependent ρ_{ab} at various fields perpendicular and parallel to the ab plane, respectively. The superconducting transition broadens and shifts toward lower temperatures by increasing fields, due to a field-induced pair breaking effect. The upper critical fields for $H//ab$ (H_{c2}^{ab}) and $H//c$ (H_{c2}^{c}) versus $T_c^{50\%}$ are summarized in Fig. 2(f), which exhibits an upward curvature. Similar features were reported in $PbTaSe_2$ [50] and $PbTaS_2$ [32], in which the upward feature was roughly fitted by

$$H_{(c2)}(t) = H_{(c2)}(0)(1 - t^{3/2})^{3/2}, \tag{1}$$

where $t = T/T_c$. Equation (1) arises from a local-pairing mechanism [51], however, which does not fit our data well.

An alternative interpretation of the upward feature suggests that $Pb_{1/3}TaS_2$ has multigap nature, as in MgB_2 [52,53], $NbSe_2$ [54], and some iron-based superconductors [55–57]. As seen in Fig. 2(f), the data are well fitted by a two-gap model [58]:

$$a_0[lnt + U(h)][lnt + U(\eta h)] + a_1[lnt + U(h)] + a_2[lnt + U(\eta h)] = 0, \tag{2}$$

where $t = T/T_c$ and $h = H_{c2}D_1/(2\phi_0/T)$ is the reduced temperature and critical field, in which $a_0 = 2(\lambda_{11}\lambda_{22} - \lambda_{12}\lambda_{21})$, $a_1 = 1 + (\lambda_{11} - \lambda_{22})/\lambda_0$, $a_2 = 1 - (\lambda_{11} - \lambda_{22})/\lambda_0$, $\lambda_0 = [(\lambda_{11} - \lambda_{22})^2 + 4\lambda_{12}\lambda_{21}]^{1/2}$, $\eta = D_2/D_1$, and $U(x) = \psi(1/2 + x) - \psi(1/2)$. λ_{11} (λ_{22}) and $\lambda_{12}(\lambda_{21})$ are the intraband and interband BCS coupling constants, respectively, $\psi(x)$ is the digamma function, and D_1 and D_2 are the diffusivity of each band. The fit parameters are listed in Table S1 (see the Supplemental Material [48]).

According to the fitting, the upper critical fields at zero-T $H_{c2}^{ab}(0)$ and $H_{c2}^{c}(0)$ are estimated to be 6.84 and 0.4 T, respectively. The in-plane $H_{c2}^{ab}(0)$ slightly exceeds the Pauli paramagnetic limit [$\mu_0 H_P^{BCS}(0) = 1.84\ T_c \approx 5.15$ T]. Subsequently, the superconducting coherence length is calculated to be $\xi_{ab}(0) \approx 28.7$ nm and $\xi_c(0) \approx 1.68$ nm through the Ginzburg-Landau (GL) formula: $H_{c2}^{c} = \Phi_0/2\pi\xi_{ab}^2$ and $H_{c2}^{ab} = \Phi_0/2\pi\xi_{ab}\xi_c$. Interestingly, $\xi_c(0)$ is close to the lattice constant. Moreover, the superconducting anisotropy ($\gamma_{H_{c2}} = H_{c2}^{ab}/H_{c2}^{c}$) is as large as 17.1, larger than that in $2H$-TaS_2 (6.7) [59], which is consistent with the fact that the distance between adjacent TaS_2 blocks is 7.42 Å for $Pb_{1/3}TaS_2$, larger than 6.05 Å of $2H$-TaS_2 [60]. Above all, the results indicate the q-2D superconducting nature in $Pb_{1/3}TaS_2$.

In order to gain further information of the superconducting state, the isothermal magnetization $M(H)$ with field along the ab plane is presented in Fig. 3(a) at various temperatures. The inset shows the full magnetization loop at 1.8 K, indicating $Pb_{1/3}TaS_2$ is a typical type-II superconductor.

The in-plane lower critical field H_{c1}^{ab} can be determined at the point which the magnetization curve starts to deviate from the linear Meissner response. H_{c1}^{ab} versus T is plotted in Fig. 3(b), which is fitted by the conventional formula

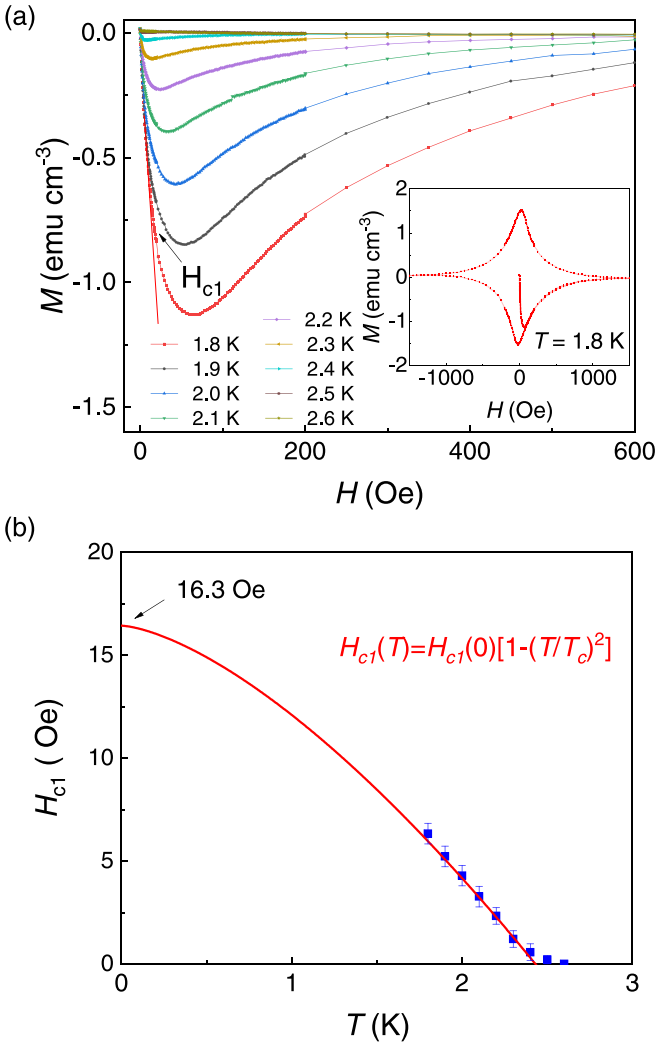

FIG. 3. (a) Magnetization $M(H)$ curves at various temperatures of $Pb_{1/3}TaS_2$ single crystal; the inset shows the loop taken at 1.8 K. (b) The superconducting H-T phase diagram of $Pb_{1/3}TaS_2$.

$H_{c1}(T) = H_{c1}(0)[1-(T/T_c)^2]$ for a weakly coupled superconductor [61]. H_{c1}^{ab} at zero-T is estimated to be 16.3 Oe.

Using the relationship $H_{c2}^{ab}(0)/H_{c1}^{ab}(0) = 2\kappa_{ab}^2/ln\kappa_{ab}$ and $\kappa_{ab}(0) = \lambda_{ab}(0)/\xi_c(0)$, we estimate the GL parameter $\kappa_{ab} \approx 98.1$ and penetration depth $\lambda_{ab}(0) \approx 164.8$ nm, the resulted parameters are summarized in Table I for brevity, indicating

TABLE I. The anisotropic superconducting parameters of $Pb_{1/3}TaS_2$ single crystal.

Parameters	Values (unit)
$H_{c2}^{ab}(0)$	6.84 (T)
$H_{c2}^{c}(0)$	0.4 (T)
$\xi_{ab}(0)$	28.7 (nm)
$\xi_c(0)$	1.68 (nm)
$H_{c1}^{ab}(0)$	16.3 (Oe)
$\lambda_{ab}(0)$	164.8 (nm)
κ_{ab}	98.1
$\gamma_{H_{c2}}$	17.1

$Pb_{1/3}TaS_2$ is an extreme type-II superconductor with highly anisotropic properties.

Now we report the topological electronic bands of the $Pb_{1/3}TaS_2$ system predicted by our first-principles calculations. Figure 4(a) presents the electronic band structure of $Pb_{1/3}TaS_2$ in the presence of SOC, with high-symmetry k points given in Fig. 4(b). Six isolated bands (numbered as band 1 to 6 from low to high energy) are located in the vicinity of the Fermi energy. Each band has double degeneracy (Kramers pair) because of the $\mathcal{PT}$ symmetry. The band dispersion along the k_z direction (i.e., A-Γ, K-H) is relatively weak in comparison to that along the in-plane direction (i.e., A-L-H-A, Γ-M-K), indicating the q-2D of the material, in agreement with the experimental observation.

For further analysis, it is essential to list the crystalline symmetries in $Pb_{1/3}TaS_2$ that are of particular importance: three vertical mirrors $\mathcal{M}_{[1\bar{1}0]} = \{\bar{2}[1\bar{1}0]|0,0,0\}$, $\mathcal{M}_{[120]} = \{\bar{2}[120]|0,0,0\}$, $\mathcal{M}_{[210]} = \{\bar{2}[210]|0,0,0\}$; a horizontal mirror $\mathcal{M}_{[001]} = \{\bar{2}[001]|0,0,\frac{1}{2}\}$; a threefold rotation $\mathcal{C}_{3[001]} = \{3[001]|0,0,0\}$; and a sixfold screw $\widetilde{\mathcal{C}}_{6[001]} = \{6[001]|0,0,\frac{1}{2}\}$. In combination with vertical mirrors and the $\mathcal{PT}$ symmetry, $\mathcal{M}_{[001]}$ nonsymmorphically dictates multiple Dirac nodal lines on the $k_z = \pi$ plane [colored by blue in Fig. 4(b)] for every two bands [23,24]. We refer to the nodal lines between bands 1 and 2 as NL1, similarly for NL2 and NL3, as illustrated in Fig. 4(a). Crossing bands for each nodal line are distinguished by opposite $\mathcal{M}_{[001]}$ eigenvalues (i or $-i$) as shown in Fig. 4(a). A detailed argument can be found in Supplemental Material [48]. Apart from the symmetry-enforced degeneracies, an accidental $\mathcal{M}_{[001]}$-protected nodal line (NL4) exists between bands 5 and 6 [Figs. 4(a) (left inset) and 4(b)]. As stabilized by the mirror $\mathcal{M}_{[001]}$, each line node in NL1-4 is shown to carry a zero-dimensional topological charge $Q = 1$ [23], confirming the nontrivial topology of above nodal lines.

Along with the line degeneracies, Figs. 4(a) and 4(b) reveal two sets of Dirac points on the rotation and screw axes A-Γ and K-H, denoted as DP1 and DP2, with the stability guaranteed by the sixfold screw $\widetilde{\mathcal{C}}_{6[001]}$ and threefold rotation $\mathcal{C}_{3[001]}$, respectively. If 2% compression along the b axis breaks $\mathcal{C}_{3[001]}$ and consequently opens up DP2, the crossing bands (bands 4 and 5) will become fully gapped, leading to a $\mathbb{Z}_2 = 1$ (see the Supplemental Material for details [48]). Therefore, topological surface states will emerge between bands 4 and 5 [3], as discussed below.

By constructing a semi-infinite (001) slab with the Pb termination, we demonstrate the momentum-resolved surface density of states (DOS) of $Pb_{1/3}TaS_2$ in Fig. 4(c). High-symmetry points in the reduced surface BZ are given in Fig. 4(b). Surface states and the corresponding bulk line or point nodes are labeled. Along the $\bar{M}$-$\bar{\Gamma}$-$\bar{M}$ path [left panel of Fig. 4(c)], surface states related to DP1, DP2, and NL3 are observed in turn from low to high energy. The surface band SS'2 is particularly illustrated in the left enlarged view of Fig. 4(c). SS'2 consistently appears even if DP2 is opened up by a symmetry breaking (e.g., compression along the b axis), because of the inverted band structure and the resulting $\mathbb{Z}_2$ invariant 1. Along the $\bar{K}$-$\bar{X}_1$-$\bar{K}$ direction [right panel of Fig. 4(c)], line nodes responsible for NL1, NL2, and NL3, as well as the induced boundary modes are emergent.

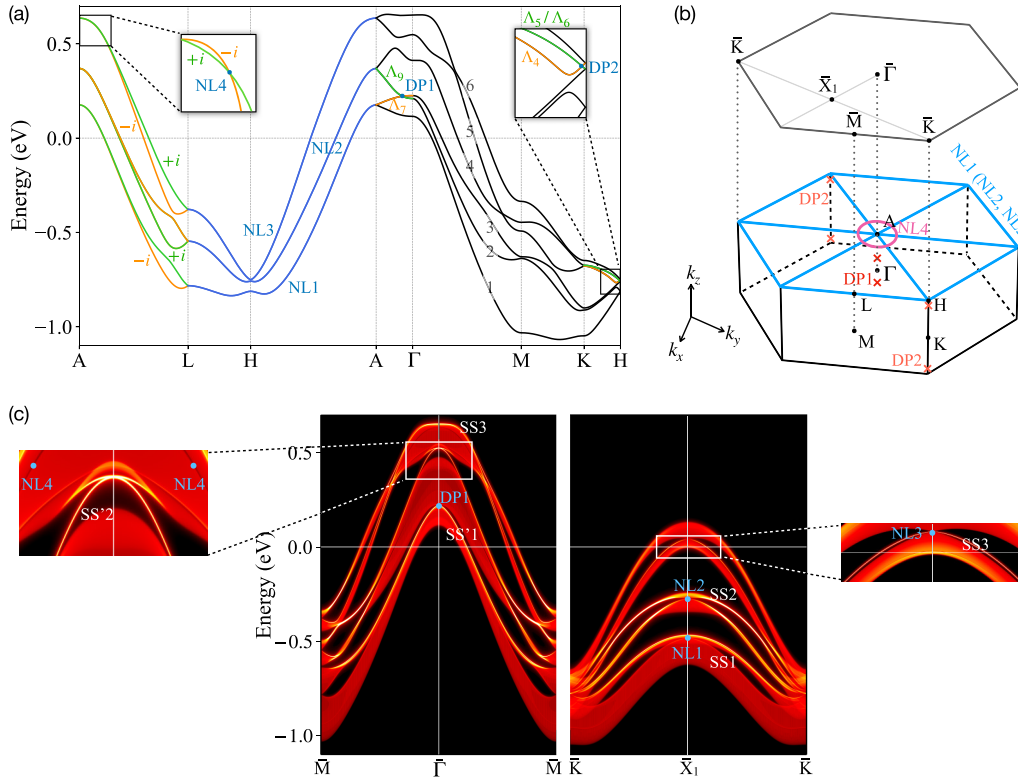

FIG. 4. Electronic structure of $Pb_{1/3}TaS_2$. (a) Electronic bands along a high-symmetry path. Energy is measured from the Fermi level. Orange and green distinguish crossing bands with different symmetry operation eigenvalues or irreducible representations (IRs). Dirac line and point degeneracies are labeled and highlighted in blue. Note that along the Γ-*M*-*K*-*H* line, all the seemingly gap closings are actually open at the meV scale except for DP2 and those at point *H*. Insets display enlarged views of the band structure. The band gap in the left inset is exaggerated to enhance the visibility. (b) Brillouin zone (BZ) and surface BZ of $Pb_{1/3}TaS_2$. High-symmetry points are marked. Dirac nodal lines and points are indicated. (c) Momentum-resolved densities of states (DOS) of a semi-infinite (001) Pb-terminated slab. Yellow and dark red correspond to high and low densities, respectively. The bulk nodes as well as surface states are highlighted.

We note that NL4 is covered by the high-intensity surface modes from NL3 and therefore is invisible in the surface spectrum.

Although many candidates of NLSMs have been proposed, experimental realizations of NLSMs are still relatively scarce [17,62]. One of the biggest challenges is that the most of the NLSMs theoretically predicted are fragile to SOC (e.g., $PbTaS_2$ [32] and $SnTaS_2$ [33]). In our study, we have proposed a new TCM $Pb_{1/3}TaS_2$ hosting nodal-line structures, which remain stable even under significant SOC by virtue of the nonsymmorphic symmetry protection, and hence can be observed in a realistic experiment. Remarkably, $Pb_{1/3}TaS_2$ also possesses multiple Dirac points that can be driven into a TI phase by breaking the rotation symmetry. We predict Dirac-cone-like surface modes on the (001) surface, owing to the nontrivial band topology. Moreover, the q-2D feature and anisotropic transport are also supported by the band dispersions. Our results signify that $Pb_{1/3}TaS_2$ could act as a prospective platform to study the interaction between topological property and superconductivity. For the future work, angle-resolved photoemission spectroscopy (ARPES) and scanning tunneling microscopy (STM) studies are needed to identify the band structure and superconducting gap directly.

IV. CONCLUSION

In summary, from first-principles calculations, the centrosymmetric $Pb_{1/3}TaS_2$ manifests multiple nodal states along with Dirac-cone-like surface states in the presence of SOC. Additionally, our experimental results suggest q-2D superconductivity with highly anisotropic features in this system. The combination of nontrivial band topology and superconductivity makes $Pb_{1/3}TaS_2$ a candidate for further research of TSCs. Our work presents an important breakthrough in searching for new topological phases by building blocks design based on symmetry analysis.

ACKNOWLEDGMENTS

The authors are grateful to Chao Cao, Wei Zhu, and Takuya Nomoto for helpful discussion. C.X. acknowledges the computational resources at the HPC center at Hangzhou Normal University in China and the RIKEN Center in Japan. This research was supported by the National Natural Science Foundation of China via Projects No. 11904294 and No. 11774305, National Key Projects for Research and Development of China (Grant No. 2019YFA0308602), Zhejiang Provincial Natural Science Foundation of China under Grant

No. LQ19A040005, and the foundation of Westlake Multidisciplinary Research Initiative Center (MRIC) (Grant No. MRIC20200402). M.H. acknowledges the support from JST CREST (Grant No. JPMJCR19T2). The authors are thankful for the support provided by Xiaohe Miao and Lin Liu from Instrumentation and Service Center for Physical Sciences at Westlake University.

X.Y. and T.Y. contributed equally to this work.

[1] Y. L. Chen, J. G. Analytis, J.-H. Chu, Z. K. Liu, S.-K. Mo, X. L. Qi, H. J. Zhang, D. H. Lu, X. Dai, Z. Fang, S. C. Zhang, I. R. Fisher, Z. Hussain, and Z.-X. Shen, Science **325**, 178 (2009).

[2] J. E. Moore, Nature (London) **464**, 194 (2010).

[3] M. Z. Hasan and C. L. Kane, Rev. Mod. Phys. **82**, 3045 (2010).

[4] Y. Ando, J. Phys. Soc. Jpn. **82**, 102001 (2013).

[5] Z. K. Liu, B. Zhou, Y. Zhang, Z. J. Wang, H. M. Weng, D. Prabhakaran, S.-K. Mo, Z. X. Shen, Z. Fang, X. Dai, Z. Hussain, and Y. L. Chen, Science **343**, 864 (2014).

[6] B. Q. Lv, H. M. Weng, B. B. Fu, X. P. Wang, H. Miao, J. Ma, P. Richard, X. C. Huang, L. X. Zhao, G. F. Chen, Z. Fang, X. Dai, T. Qian, and H. Ding, Phys. Rev. X **5**, 031013 (2015).

[7] S. Borisenko, D. Evtushinsky, Q. Gibson, A. Yaresko, K. Koepernik, T. Kim, M. Ali, J. van den Brink, M. Hoesch, A. Fedorov, E. Haubold, Y. Kushnirenko, I. Soldatov, R. Schäfer, and R. J. Cava, Nat. Commun. **10**, 3424 (2019).

[8] G. Bian, T.-R. Chang, R. Sankar, S.-Y. Xu, H. Zheng, T. Neupert, C.-K. Chiu, S.-M. Huang, G. Chang, I. Belopolski, D. S. Sanchez, M. Neupane, N. Alidoust, C. Liu, B. Wang, C.-C. Lee, H.-T. Jeng, C. Zhang, Z. Yuan, S. Jia, A. Bansil, F. Chou, H. Lin, and M. Z. Hasan, Nat. Commun. **7**, 10556 (2016).

[9] M. Neupane, I. Belopolski, M. M. Hosen, D. S. Sanchez, R. Sankar, M. Szlawska, S.-Y. Xu, K. Dimitri, N. Dhakal, P. Maldonado, P. M. Oppeneer, D. Kaczorowski, F. Chou, M. Z. Hasan, and T. Durakiewicz, Phys. Rev. B **93**, 201104(R) (2016).

[10] X. Wan, A. M. Turner, A. Vishwanath, and S. Y. Savrasov, Phys. Rev. B **83**, 205101 (2011).

[11] Z. Wang, Y. Sun, X.-Q. Chen, C. Franchini, G. Xu, H. Weng, X. Dai, and Z. Fang, Phys. Rev. B **85**, 195320 (2012).

[12] A. A. Burkov, M. D. Hook, and L. Balents, Phys. Rev. B **84**, 235126 (2011).

[13] S. M. Young, S. Zaheer, J. C. Y. Teo, C. L. Kane, E. J. Mele, and A. M. Rappe, Phys. Rev. Lett. **108**, 140405 (2012).

[14] A. Burkov, Nat. Mater. **15**, 1145 (2016).

[15] M. Hirayama, R. Okugawa, T. Miyake, and S. Murakami, Nat. Commun. **8**, 14022 (2017).

[16] M. Hirayama, R. Okugawa, and S. Murakami, J. Phys. Soc. Jpn. **87**, 041002 (2018).

[17] J. Fujioka, R. Yamada, M. Kawamura, S. Sakai, M. Hirayama, R. Arita, T. Okawa, D. Hashizume, M. Hoshino, and Y. Tokura, Nat. Commun. **10**, 362 (2019).

[18] R. Yamada, J. Fujioka, M. Kawamura, S. Sakai, M. Hirayama, R. Arita, T. Okawa, D. Hashizume, M. Hoshino, and Y. Tokura, Phys. Rev. Lett. **123**, 216601 (2019).

[19] R. A. Molina and J. González, Phys. Rev. Lett. **120**, 146601 (2018).

[20] N. B. Kopnin, T. T. Heikkilä, and G. E. Volovik, Phys. Rev. B **83**, 220503(R) (2011).

[21] S. M. Young and C. L. Kane, Phys. Rev. Lett. **115**, 126803 (2015).

[22] C. Fang, Y. Chen, H.-Y. Kee, and L. Fu, Phys. Rev. B **92**, 081201(R) (2015).

[23] B.-J. Yang, T. A. Bojesen, T. Morimoto, and A. Furusaki, Phys. Rev. B **95**, 075135 (2017).

[24] S. Li, Y. Liu, S.-S. Wang, Z.-M. Yu, S. Guan, X.-L. Sheng, Y. Yao, and S. A. Yang, Phys. Rev. B **97**, 045131 (2018).

[25] Y. Chen, Y.-M. Lu, and H.-Y. Kee, Nat. Commun. **6**, 6593 (2015).

[26] P.-J. Chen, T.-R. Chang, and H.-T. Jeng, Phys. Rev. B **94**, 165148 (2016).

[27] G. Bian, T.-R. Chang, H. Zheng, S. Velury, S.-Y. Xu, T. Neupert, C.-K. Chiu, S.-M. Huang, D. S. Sanchez, I. Belopolski, N. Alidoust, P.-J. Chen, G. Chang, A. Bansil, H.-T. Jeng, H. Lin, and M. Z. Hasan, Phys. Rev. B **93**, 121113(R) (2016).

[28] Y. Li, Y. Wu, X. Chenchao, N. Liu, Jiang, B. Lv, Y. Gang, Y. Liu, H. Bai, X. Yang, L. Qiao, M. Li, L. Li, H. Xing, Y. Huang, J. Ma, M. Shi, C. Cao, Y. Liu, C. Liu, J. Jia, and Z.-A. Xu, Sci. Bull. **66**, 243 (2021).

[29] Y. Li, Z. Wu, J. Zhou, K. Bu, C. Xu, L. Qiao, M. Li, H. Bai, J. Ma, Q. Tao, C. Cao, Y. Yin, and Z.-A. Xu, Phys. Rev. B **102**, 224503 (2020).

[30] Y. Du, X. Bo, D. Wang, E.-J. Kan, C.-G. Duan, S. Y. Savrasov, and X. Wan, Phys. Rev. B **96**, 235152 (2017).

[31] S. Y. Guan, P. J. Chen, M. W. Chu, R. Sankar, F. Chou, H. T. Jeng, C. S. Chang, and T. M. Chuang, Sci. Adv. **2**, e1600894 (2016).

[32] J. J. Gao, J. G. Si, X. Luo, J. Yan, Z. Z. Jiang, W. Wang, C. Q. Xu, X. F. Xu, P. Tong, W. H. Song, X. B. Zhu, W. J. Lu, and Y. P. Sun, J. Phys. Chem. C **124**, 6349 (2020).

[33] D.-Y. Chen, Y. Wu, L. Jin, Y. Li, X. Wang, J. X. Duan, J. Han, X. Li, Y.-Z. Long, X. Zhang, D. Chen, and B. Teng, Phys. Rev. B **100**, 064516 (2019).

[34] G. Kresse and J. Furthmüller, Phys. Rev. B **54**, 11169 (1996).

[35] J. P. Perdew, K. Burke, and M. Ernzerhof, Phys. Rev. Lett. **77**, 3865 (1996).

[36] J. Gao, Q. Wu, C. Persson, and Z. Wang, Comp. Phys. Commun **261**, 107760 (2021).

[37] N. Marzari and D. Vanderbilt, Phys. Rev. B **56**, 12847 (1997).

[38] I. Souza, N. Marzari, and D. Vanderbilt, Phys. Rev. B **65**, 035109 (2001).

[39] G. Pizzi, V. Vitale, R. Arita, S. Blügel, F. Freimuth, G. Géranton, M. Gibertini, D. Gresch, C. Johnson, T. Koretsune, J. Ibañez-Azpiroz, H. Lee, J.-M. Lihm, D. Marchand, A. Marrazzo, Y. Mokrousov, J. I. Mustafa, Y. Nohara, Y. Nomura, L. Paulatto, S. Poncé, T. Ponweiser, J. Qiao, F. Thöle, S. S. Tsirkin, M. Wierzbowska, N. Marzari, D. Vanderbilt, I. Souza, A. A. Mostofi, and J. R. Yates, J. Phys.: Condens. Matter **32**, 165902 (2020).

[40] Q. Wu, S. Zhang, H.-F. Song, M. Troyer, and A. A. Soluyanov, Comput. Phys. Commun. **224**, 405 (2018).

[41] M. P. L. Sancho, J. M. L. Sancho, J. M. L. Sancho, and J. Rubio, J. Phys. F: Met. Phys. **15**, 851 (1985).

[42] V. Wang, N. Xu, J. Liu, G. Tang, and W. Geng, Comp. Phys. Commun. **267**, 108033 (2021).
[43] K. Momma and F. Izumi, J. Appl. Cryst. **41**, 653 (2008).
[44] W. Setyawan and S. Curtarolo, Comp. Mater. Sci **49**, 299 (2010).
[45] A. Togo and I. Tanaka, arXiv:1808.01590.
[46] C. M. Fang, G. A. Wiegers, A. Meetsma, R. A. De Groot, and C. Haas, Physica B (Amsterdam, Neth.) **226**, 259 (1996).
[47] H. Katzke, P. Tolédano, and W. Depmeier, Phys. Rev. B **69**, 134111 (2004).
[48] See Supplemental Material at http://link.aps.org/supplemental/10.1103/PhysRevB.104.035157 for details of EDX pattern, the parameters of two-band model, symmetry-enforced nodal lines, and the band structure of $Pb_{1/3}TaS_2$ under compression.
[49] S. Nagata, T. Aochi, T. Abe, S. Ebisu, T. Hagino, Y. Seki, and K. Tsutsumi, J. Phys. Chem. Solids **53**, 1259 (1992).
[50] M. N. Ali, Q. D. Gibson, T. Klimczuk, and R. J. Cava, Phys. Rev. B **89**, 020505(R) (2014).
[51] R. Micnas, J. Ranninger, and S. Robaszkiewicz, Rev. Mod. Phys. **62**, 113 (1990).
[52] M. Iavarone, G. Karapetrov, A. E. Koshelev, W. K. Kwok, G. W. Crabtree, D. G. Hinks, W. N. Kang, E.-M. Choi, H. J. Kim, H.-J. Kim, and S. I. Lee, Phys. Rev. Lett. **89**, 187002 (2002).
[53] A. Gurevich, Physica C (Amsterdam, Neth.) **456**, 160 (2007).
[54] A. Majumdar, D. VanGennep, J. Brisbois, D. Chareev, A. V. Sadakov, A. S. Usoltsev, M. Mito, A. V. Silhanek, T. Sarkar, A. Hassan, O. Karis, R. Ahuja, and M. Abdel-Hafiez, Phys. Rev. Mater. **4**, 084005 (2020).
[55] X. Xing, W. Zhou, J. Wang, Z. Zhu, Y. Zhang, N. Zhou, B. Qian, X. Xu, and Z. Shi, Sci. Rep. **7**, 45943 (2017).
[56] H.-S. Lee, M. Bartkowiak, J.-H. Park, J.-Y. Lee, J.-Y. Kim, N.-H. Sung, B. K. Cho, C.-U. Jung, J. S. Kim, and H.-J. Lee, Phys. Rev. B **80**, 144512 (2009).
[57] M. Kano, Y. Kohama, D. Graf, F. Balakirev, A. S. Sefat, M. A. Mcguire, B. C. Sales, D. Mandrus, and S. W. Tozer, J. Phys. Soc. Jpn. **78**, 084719 (2009).
[58] A. Gurevich, Phys. Rev. B **67**, 184515 (2003).
[59] R. C. Morris and R. V. Coleman, Phys. Rev. B **7**, 991 (1973).
[60] R. Eppinga and G. A. Wiegers, Physica B (Amsterdam, Neth.) **99**, 121 (1980).
[61] J. P. Carbotte, Rev. Mod. Phys. **62**, 1027 (1990).
[62] C. Chen, X. Xu, J. Jiang, S.-C. Wu, Y. P. Qi, L. X. Yang, M. X. Wang, Y. Sun, N. B. M. Schröter, H. F. Yang, L. M. Schoop, Y. Y. Lv, J. Zhou, Y. B. Chen, S. H. Yao, M. H. Lu, Y. F. Chen, C. Felser, B. H. Yan, Z. K. Liu, and Y. L. Chen, Phys. Rev. B **95**, 125126 (2017).